Resonant modes of 12-fold symmetric defect free photonic quasicrystal

Minfeng Chen,[1] Yun-Jing Li,[3] Yuh-Jen Cheng,*[1,2] Yai-Chung Chang,[1,2] and Chun-Yen Chang[3]

[1]*Research Center for Applied Sciences, Academia Sinica, 128 Sec. 2, Academia Rd, Nankang, Taipei 115, Taiwan*
[2]*Department of Photonics, National Chiao Tung University, 1001 Ta Hsueh Rd. Hsinchu 300, Taiwan*
[3]*Institute of Electro-Optical Engineering, National Chiao Tung University, 1001 Ta Hsueh Rd., Hsinchu 300, Taiwan*
*yjcheng@sinica.edu.tw

Abstract: This work investigates the resonant modes of a 12-fold symmetric defect free photonic quasicrystal (PQC) nanorod array using finite difference time domain (FDTD) simulation. Localized modes can exist in PQC without introducing defects due to the lack of translational symmetry. The resonant modes of the unit cell PQC and the one time expanded PQC from unit cell are systematically examined. The resonant spectrum is that of a single rod modified by the interaction among PQC nanorods. The mode confinement is contributed by guided resonance and destructive interference scattering. The self-scaling similarity of resonant spectrum and mode profile are also investigated.

OCIS codes: (160.5298) Photonic crystals; (030.4070) Modes.

References and links

1. M. Kohmoto, B. Sutherland, and K. Iguchi, "Localization of optics: quasiperiodic media," Phys. Rev. Lett. **58**(23), 2436–2438 (1987).
2. W. Gellermann, M. Kohmoto, B. Sutherland, and P. C. Taylor, "Localization of light waves in Fibonacci dielectric multilayers," Phys. Rev. Lett. **72**(5), 633–636 (1994).
3. T. Hattori, N. Tsurumachi, S. Kawato, and H. Nakatsuka, "Photonic dispersion relation in a one-dimensional quasicrystal," Phys. Rev. B Condens. Matter **50**(6), 4220–4223 (1994).
4. L. Dal Negro, C. J. Oton, Z. Gaburro, L. Pavesi, P. Johnson, A. Lagendijk, R. Righini, M. Colocci, and D. S. Wiersma, "Light transport through the band-edge states of Fibonacci quasicrystals," Phys. Rev. Lett. **90**(5), 055501 (2003).
5. W. Man, M. Megens, P. J. Steinhardt, and P. M. Chaikin, "Experimental measurement of the photonic properties of icosahedral quasicrystals," Nature **436**(7053), 993–996 (2005).
6. A. Ledermann, L. Cademartiri, M. Hermatschweiler, C. Toninelli, G. A. Ozin, D. S. Wiersma, M. Wegener, and G. von Freymann, "Three-dimensional silicon inverse photonic quasicrystals for infrared wavelengths," Nat. Mater. **5**(12), 942–945 (2006).
7. T. Matsui, A. Agrawal, A. Nahata, and Z. V. Vardeny, "Transmission resonances through aperiodic arrays of subwavelength apertures," Nature **446**(7135), 517–521 (2007).
8. S. Walter and S.-W. Daniel, "Photonic and phononic quasicrystals," J. Phys. D Appl. Phys. **40**(13), R229–R247 (2007).
9. K. Mnaymneh and R. C. Gauthier, "Mode localization and band-gap formation in defect-free photonic quasicrystals," Opt. Express **15**(8), 5089–5099 (2007).
10. G. Gumbs and M. K. Ali, "Dynamical maps, Cantor spectra, and localization for Fibonacci and related quasiperiodic lattices," Phys. Rev. Lett. **60**(11), 1081–1084 (1988).
11. M. Notomi, H. Suzuki, T. Tamamura, and K. Edagawa, "Lasing Action due to the Two-Dimensional Quasiperiodicity of Photonic Quasicrystals with a Penrose Lattice," Phys. Rev. Lett. **92**(12), 123906 (2004).
12. M. E. Zoorob, M. D. B. Charlton, G. J. Parker, J. J. Baumberg, and M. C. Netti, "Complete photonic bandgaps in 12-fold symmetric quasicrystals," Nature **404**(6779), 740–743 (2000).
13. K. Nozaki and T. Baba, "Lasing Characteristics of 12-Fold Symmetric Quasi-periodic Photonic Crystal Slab Nanolasers," Jpn. J. Appl. Phys. **45**(8A), 6087–6090 (2006).
14. K. Nozaki and T. Baba, "Quasiperiodic photonic crystal microcavity lasers," Appl. Phys. Lett. **84**(24), 4875–4877 (2004).
15. J. Hendrickson, B. C. Richards, J. Sweet, G. Khitrova, A. N. Poddubny, E. L. Ivchenko, M. Wegener, and H. M. Gibbs, "Excitonic polaritons in Fibonacci quasicrystals," Opt. Express **16**(20), 15382–15387 (2008).
16. L. Mahler, A. Tredicucci, F. Beltram, C. Walther, J. Faist, H. E. Beere, D. A. Ritchie, and D. S. Wiersma, "Quasi-periodic distributed feedback laser," Nat. Photonics **4**(3), 165–169 (2010).

#197862 - $15.00 USD Received 17 Sep 2013; revised 13 Dec 2013; accepted 7 Jan 2014; published 23 Jan 2014

17. S.-K. Kim, J.-H. Lee, S.-H. Kim, I.-K. Hwang, Y.-H. Lee, and S.-B. Kim, "Photonic quasicrystal single-cell cavity mode," Appl. Phys. Lett. **86**(3), 031101 (2005).
18. S. P. Chang, K. P. Sou, C. H. Chen, Y. J. Cheng, J. K. Huang, C. H. Lin, H. C. Kuo, C. Y. Chang, and W. F. Hsieh, "Lasing action in gallium nitride quasicrystal nanorod arrays," Opt. Express **20**(11), 12457–12462 (2012).
19. M. Oxborrow and C. L. Henley, "Random square-triangle tilings: A model for twelvefold-symmetric quasicrystals," Phys. Rev. B Condens. Matter **48**(10), 6966–6998 (1993).
20. S. G. Johnson, S. Fan, P. R. Villeneuve, J. D. Joannopoulos, and L. Kolodziejski, "Guided modes in photonic crystal slabs," Phys. Rev. B **60**(8), 5751–5758 (1999).

1. Introduction

Photonic quasicrystals (PQCs) have generated substantial research interests due to their fascinating properties [1–9]. Unlike photonic crystals, PQCs do not have a periodic structure but follows simple deterministic generation rules. The generated patterns have a long range order and lie somewhere between disorder and periodic structures. They have a high level of rotational symmetry which periodic structures cannot have. Due to the lack of translational symmetry, PQCs do not support extended Bloch waves as in photonic crystals (PCs). The optical modes are critically localized, which means modes are confined in space but decay more weakly than exponentially [10]. Another interesting property of PQC structures is their scaling symmetry, in which the basic quasicrystal pattern repeats itself as the size of the structure expands by geometric scaling factors. There have been interests in exploring the use of PQCs in microcavity and distributed feedback laser applications [11–17]. Lasing can be observed from optically focused pumped PQCs without the need of introducing defects [11–18]. This is because localized modes inherently exist in PQCs. The resonant modes of PQC can have fairly complicated mode patterns and resonant peak distribution, which have not been well explored.

Here we report a systematic study of the resonant modes of a 12-fold symmetric defect free PQC. We are interested in the spectral structure and mode pattern. Conventionally, air holes are often placed at the vertices of a lattice pattern. We place pillars at the vertices instead. This allows us to study the changes of the mode field as the structure expands from a single rod to various PQC sizes. We have also investigated the mode localization and scaling symmetry property.

2. Structure model

Figure 1(a) illustrates the lattice structure of the 12 fold symmetric PQC. It is composed by the vertices of a square-triangle tiling, which is generated from a dodecagonal seed structure by using the Stamfli inflation rule [19]. The dodecagonal seed structure (unit cell) is shown in Fig. 1(a), marked in black circle. The seed structure is then expanded by an inflation factor of $2+\sqrt{3}$, as show in the dashed red lines. The unit cell is duplicated at each vertex of the inflated dashed red lines. For the convenience of reference, we call this one time expanded structure the first off-spring cell. Figure 1(a) shows a partially filled first off-spring cell, where unit cell has not been duplicated at the most outer vertices. The scaling similarity is inherent in the construction rule as can be seen by comparing the dashed red lines and the blue-line unit cell at the center. The square-triangle tiled dodecagon structure repeats itself as the size expands by the inflation factor. The construction can be iterated till filling the desired space. Figure 1(b) is a schematic of the unit cell with hexagonal pillars placed at the vertices, which consists of 1 central rod + 6 surrounding rods + 12 outer most rods. The dots are the point sources used in simulation to excite the resonant modes of the PQC. The two additional pillars added at the top are only for illustration purpose to describe a point source (4) used in resonant mode calculation for the first off-spring cell. The hexagon is chosen due to the natural crystalline structure of the GaN material used to fabricate a PQC sample. The sample was fabricated from a GaN substrate by patterned top-down etch and epitaxial regrowth [18]. Multiple quantum wells (MQWs) were grown on the nanorod surface. The photoluminescent (PL) emission of MQWs is around 460 nm. Figure 1(c) shows a SEM plane view of a fabricated sample. The PQC lattice pattern is overlaid on top for visual guidance. Without the overlaid guidance, the pattern looks almost totally random.

#197862 - $15.00 USD Received 17 Sep 2013; revised 13 Dec 2013; accepted 7 Jan 2014; published 23 Jan 2014

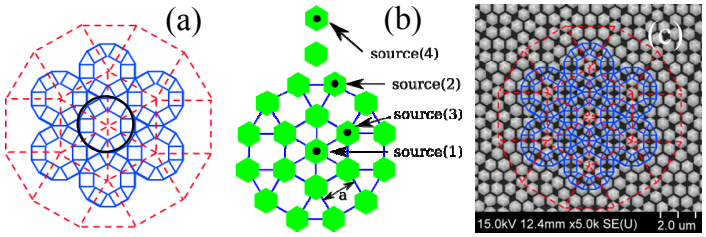

Fig. 1. (a) Construction of the 12 fold symmetric PQC structure. (b) Illustration of hexagonal rods placed at the PQC unit cell lattice vertices (blue line). Different source locations are used to excite resonant modes. (c) SEM plane view image of the fabricated sample with the PQC lattice pattern overlaid to show its PQC structure.

The dimension used in the simulation is as follows. The width of the hexagonal pillar sidewall is 340 nm. The center-to-center pillar spacing is 750 nm. The refractive index of GaN is taken to be 2.4. The fabricated pillar is about 1.2 μm in length standing on a GaN substrate. For simplicity, the simulation is carried out by two-dimensional Finite-Difference-Time-Domain (FDTD) method. Here, we are mainly interested in the general characteristics of the modes of PQC. The finite pillar length is regarded as a second order modification to the simulation results. The electric field polarized along the pillar axis is used in simulation. It is selected because the reflection for electric field parallel to pillar axis is stronger than the perpendicular one. Modes in this polarization experience a stronger confinement by the pillars and therefore are the modes of interest.

3. Simulation results and discussion

We first study the scattering properties of the PQC by calculating its reciprocal pattern, which is obtained by 2-D Fourier transform of the PQC lattice points. Here, we have only calculated finite size PQCs. The calculated results for a unit cell, the first off-spring cell, and the second off-spring cell are shown in Figs. 2(a)–2(c), respectively. The reciprocal pattern shows 12-fold rotational symmetry as expected. The pattern complexity increases dramatically as the PQC structure expands. The first off-spring cell is obtained by inflating the unit cell lattice structure and duplicating the unit cell at every vertices of the inflated structure. By the nature of this construction rule, the reciprocal pattern (Fourier transform) of the first off-spring cell is equal to that of the unit cell [(Fig. 2(a))] multiplied by the reduced copy of itself by the inflation factor. This leads to the complicated fine structures as shown in Fig. 2(b). Figure 2(b) carries similar major spots shown in Fig. 2(a), however, with additional fine structures. The same rule is also applicable to Fig. 2(c) with respect to Fig. 2(b).

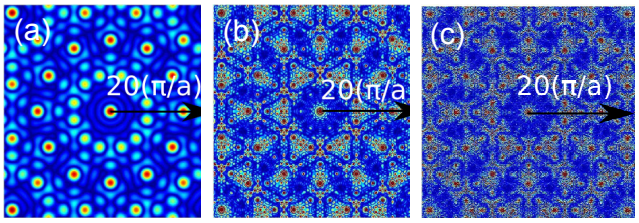

Fig. 2. The reciprocal pattern of (a) a unit cell, (b) the first off-spring cell, and (c) the second off-spring cell.

We then investigate the resonant modes of the PQC pattern. We start with a unit cell. A point source is used to probe the resonant modes and spectrum. A short Gaussian pulse width of 2 fs centered at 450 nm is launched at source locations 1, 2, 3, as shown in Fig. 1(b), and an additional one slightly offset from location 1 (not shown). The 2 fs short pulse width ensures a very broad band excitation. A long enough propagation time is used in the simulation to obtain a steady state E-field distribution. The spectrum is obtained by performing the Fourier transform of the recorded time-domain signal for both electric and

#197862 - $15.00 USD Received 17 Sep 2013; revised 13 Dec 2013; accepted 7 Jan 2014; published 23 Jan 2014

magnetic fields, followed by Poynting flux computation. Figure 3(a) shows the calculated spectra, where the blue, red, green, and gray lines are obtained from the source locations 1, 2, 3, and the offset one, respectively. The resonant peaks do not show obvious regularity. The peaks also changes for different excitation source locations. The center source 1 generates the strongest intensity peaks than the off-center sources. This is because the center source automatically satisfies the rotational symmetry of PQC, therefore can excite the resonant modes better. We consider all the distinct peaks as the resonant modes. To confirm this argument, we also carried out simulations by only changing the lattice constant to 735 and 772 nm using the center source 1. The resonant peaks redshift with increasing rod spacing, as shown in Fig. 3(b). This scaling property with lattice spacing is the evidence of QPC resonance. The change in spectral shape is because the rod dimension and the pulse were not scaled proportionally. To understand the origin of these peaks, we have also calculated the resonant spectrum of a single hexagonal rod by launching an excitation source at its center. Figure 3(c) shows the calculated spectrum. It consists of a broad resonance at 460 nm and a narrow one at 543 nm, which correspond to a fairly lossy and a well confined mode, respectively. The lossy nature of 460 nm resonance implies that it can significantly interact with the resonant modes of the surrounding rods. This results in the multiple resonant peaks around 460 nm in Fig. 3(a). The narrow 543 nm resonance on the other hand is less affected by its surrounding rods due to its well confined nature, therefore keeping its line shape almost unchanged with only very small side peaks added in Fig. 3(a). This may also explain the less position change of 543 nm peak as compared with other peaks in Fig. 3(b). The cavity quality factor of the 460 nm resonance of a single rod is 12. This Q factor is enhanced to 65 for the resonant modes in the unit cell.

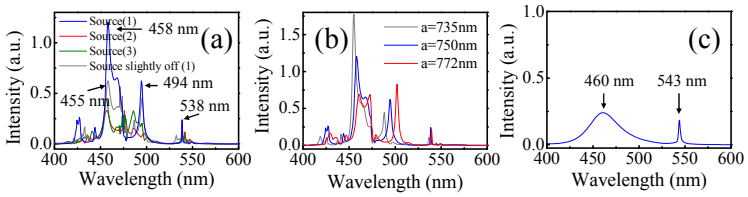

Fig. 3. The calculated resonant spectra of the unit cell obtained from (a) various source locations and (b) various lattice constants. (c) The resonant spectrum of a single rod.

To investigate the resonant mode pattern, we identify three resonant peaks excited by the center source 1, λ = 458, 494, and 538 nm, and the one excited by the source 3, λ = 455 nm. The mode patterns are obtained by injecting a narrow band signal at each peak wavelength and letting the field distribution settled after sufficient long propagation time. The mode profiles are shown in Figs. 4(a)–4(d). The resonant profiles excited by the center source 1, as shown in Figs. 4(a)–4(c), are mostly confined within the inner two layers, i.e. one central rod plus six surrounding rods. Figure 4(d) shows the 455 nm resonance excited by the off-center source 3. It has a skewed resonant pattern due to its asymmetric rod surrounding, as compared with Fig. 4(a). The mode profiles of the two resonances of the single rod spectrum in Fig. 3(c) are also calculated. The 460 nm single rod resonance shows a radial propagation pattern, as shown in Fig. 4(e). The same characteristic is also present in Figs. 4(a), 4(b), and 4(d), indicating that they are originated from the same 460 nm resonance of a single rod. The single rod resonant mode at 543 nm, as shown in Fig. 4(f), is a whispery gallery mode with high field intensity circulating around the rod boundary. The same pattern is also present in Fig. 4(c) where surrounding rods are excited with similar pattern but much lower intensity. This indicates that its origin is from the 543 nm resonance of a single rod.

#197862 - $15.00 USD Received 17 Sep 2013; revised 13 Dec 2013; accepted 7 Jan 2014; published 23 Jan 2014

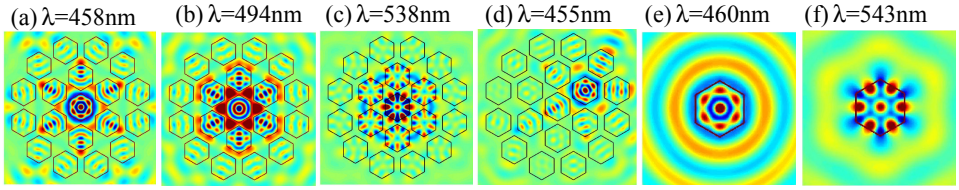

Fig. 4. (a)-(d) The mode patterns of resonant peaks 458, 494, 538, and 455 nm of the unit PQC cell. (e)-(f) The mode patterns of resonant peaks 460 and 543 nm of a single rod.

We then investigate the resonant modes of the first off-spring cells by similar approach. The calculated resonant spectrum excited by the central excitation source 1, as shown in Fig. 5(a), reveals more distinct resonant peaks as compared with that of the unit cell. The field intensity and linewidth are greatly enhanced with respect to that of the unit cell under the same excitation condition, indicative of much better field confinement. The cavity Q factor of resonance is significantly enhanced from 65 in unit cell to 540 in first off-spring cell. This is attributed to the feedbacks provided by the added outer two layers of unit cells in the first off-spring cell. The 538 nm whispering gallery mode becomes negligible as compared with other radial propagating modes. This implies that the added rods greatly enhance the confinement of the radial propagation modes while having little effect on the whispering gallery mode. Figure 5(b) plots the resonant spectra excited by various source locations shown in Fig. 1(b). Similar to the previous result, the resonant peaks are sensitive to different excitation sources. The lasing spectrum versus pump power intensity from a previous report is shown in Fig. 5(c) for qualitative comparison [18]. The lasing peaks reveal the PQC resonant modes within the MQW gain bandwidth. It shows similar irregular peak distribution but lack of peak to peak matches. The discrepancy could be due to the overly simplified 2D model and limited MQW gain bandwidth. The inclusion of propagation in normal to the substrate direction in a real 3D model will change the resonant mode locations and may change some of them into radiative modes [20]. The absence of 494 nm peak could be due to its location at edge of MQW gain bandwidth, which rolls off at 500 nm. In addition, its mode field has a significant high intensity portion located outside the rods, in particular the six red lobes surrounding the center rod as shown in Fig. 4(b). The 458 nm mode on the contrary has most of high intensity mode field located inside the rods. The 494 nm mode thus sees less model gain since rods provide the gain. This further limits its ability to reach lasing threshold.

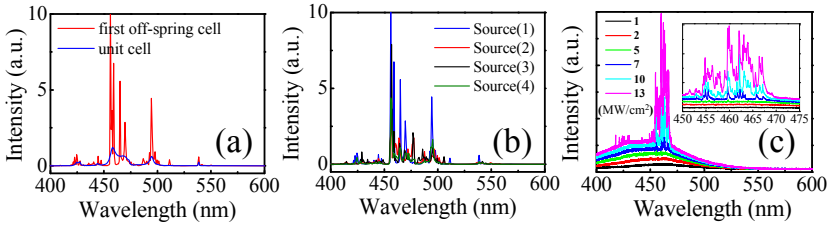

Fig. 5. (a) Resonant spectrum of the first off-spring cell. Unit cell spectrum is also included for comparison. (b) Resonant spectra of the first off-spring cell for various excitation sources. (c) Lasing spectrum when a PQC sample was pumped by a pulsed laser.

Figure 6(a) shows the mode profile of the λ = 458 nm resonance of the first off-spring cell, obtained by the same calculation approach mentioned previously. The rod contours are overlaid on the mode profile for visual reference. The dashed red line circles indicate the unit cell locations. The high intensity part is mostly confined in the center region consisting of a center rod plus surrounding six rods, as shown in the enlarged Fig. 6(b). Compared with Fig. 4(a), mode pattern similar to the unit cell is maintained. The additional six unit cells surrounding the center one provides better mode confinement by channeling the optical energy back to the center region. It is interesting to see the pseudo wave guiding effect formed by the surrounding rods. Figure 6(c) shows the mode profile of the λ = 494 nm

#197862 - $15.00 USD Received 17 Sep 2013; revised 13 Dec 2013; accepted 7 Jan 2014; published 23 Jan 2014

resonance. Figure 6(d) is its enlarged center portion. There is no pseudo wave guiding. Instead, the surrounding rods provide the mode confinement by destructive interference like random scattering.

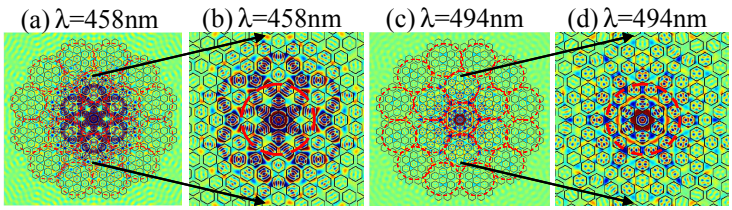

Fig. 6. (a) and (c) are the 458 nm and 494 nm resonant mode profiles of the first off-spring cells, respectively. (b) and (d) are respectively the enlarged center portion of (a) and (c). The overlaid dashed red line circles are the unit cells for visual guidance.

We now turn to the self scaling similarity property, which is inherent in the inflation construction rule. To test this property, the center wavelength of the broad band excitation source was redshifted to ~1300 nm. The results are depicted in Fig. 7. The resonant spectral pattern shown in Fig. 7(a) is similar to that of the unit cell shown in Fig. 3(a). The 1285 nm and 1398 nm peaks correspond to the 458 nm and 494 nm peaks in the unit cell, respectively. Figure 7(b) shows the calculated mode pattern of the λ = 1285 nm peak. The mode profile is similar to that of the unit cell shown in Fig. 4(a). The individual rod dimension is negligible at this wavelength. The rods collective together in a unit cell structure, denoted by the large hexagons, determines the mode pattern as individual rod does in Fig. 4(a). This demonstrates the interesting self-scaling similarity property inherent in the PQC construction rule.

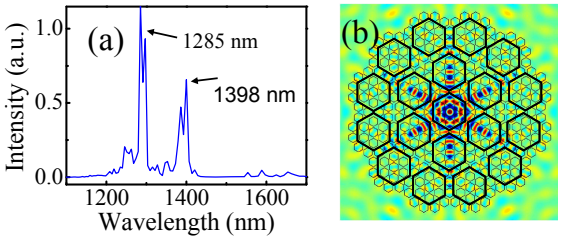

Fig. 7. (a) The calculated spectrum from 1100 to 1700 nm. (b) The calculated mode profile. The large hexagons represent the locations of unit cells.

4. Summary

PQC represents an interesting class of pattern that is between ordered and completely random structure. Localized resonant modes can exist without introducing any defect due to lack of translational symmetry. The resonant mode can be well confined in the first-offspring cell, which is just the first expansion from the unit cell. The resonant spectrum can be viewed as that of a single rod modified by the scattering interaction among rods in PQC pattern. The interaction can form pseudo wave guiding channels and destructive interference like random scattering to provide the mode confinement. The self scaling similarity inherent in the PQC construction rule is also demonstrated in the resonant mode and spectrum calculation.

Acknowledgments

We thank the National Science Council of Taiwan for the support of this research under contract NSC 100-2112-M-001-021-MY3 and Sinica nano project.